

Domain generalization in deep learning for contrast-enhanced imaging

Carla Sendra-Balcells^{a,1,*}, Víctor M. Campello^{a,1}, Carlos Martín-Isla^a, David Vilades Medel^b,
Martín Luís Descalzo^b, Andrea Guala^c, José F. Rodríguez Palomares^c, Karim Lekadir^a

^a*Dept. de Matemàtiques i Informàtica, Universitat de Barcelona, Spain*

^b*Hospital de la Santa Creu i Sant Pau, Universitat Autònoma de Barcelona, Spain*

^c*Cardiovascular Imaging Unit, Hospital Universitari Vall d'Hebron, Barcelona, Spain*

Abstract

Background: The domain generalization problem has been widely investigated in deep learning for non-contrast imaging over the last years, but it received limited attention for contrast-enhanced imaging. However, there are marked differences in contrast imaging protocols across clinical centers, in particular in the time between contrast injection and image acquisition, while access to multi-center contrast-enhanced image data is limited compared to available datasets for non-contrast imaging. This calls for new tools for generalizing single-domain, single-center deep learning models across new unseen domains and clinical centers in contrast-enhanced imaging.

Methods: In this paper, we present an exhaustive evaluation of deep learning techniques to achieve generalizability to unseen clinical centers for contrast-enhanced image segmentation. To this end, several techniques are investigated, optimized and systematically evaluated, including data augmentation, domain mixing, transfer learning and domain adaptation. To demonstrate the potential of domain generalization for contrast-enhanced imaging, the methods are evaluated for ventricular segmentation in contrast-enhanced cardiac magnetic resonance imaging (MRI).

Results: The results are obtained based on a multi-center cardiac contrast-enhanced MRI dataset acquired in four hospitals located in three countries (France, Spain and China). They show that the combination of data augmentation and transfer learning can lead to single-center models that generalize well to new clinical centers not included during training.

Conclusions: Single-domain neural networks enriched with suitable generalization procedures can reach and even surpass the performance of multi-center, multi-vendor models in contrast-enhanced imaging, hence eliminating the need for comprehensive multi-center datasets to train generalizable models.

Keywords: Deep learning, contrast-enhanced imaging, domain generalization, cardiac image segmentation, data augmentation, transfer learning.

1. Introduction

1.1. Problem and motivation

Over the last years, the domain shift problem has attracted increased attention in the medical image analysis community [1]. Several studies have evaluated the level of generalization of deep

*Corresponding author:

Email address: carla.sendra@ub.edu (Carla Sendra-Balcells)

¹Shared first authorship.

learning techniques across domains [2]. For example, a recent challenge on this topic was organized in the cardiac magnetic resonance imaging (MRI) domain at the 2020 Medical Image Computing & Computer-Assisted Intervention conference (MICCAI 2020), in collaboration with six Spanish, German and Canadian clinical centers. Entitled "Multi-Centre, Multi-Vendor and Multi-Disease Cardiac Segmentation (M&Ms)", the study demonstrated that single-center, single-vendor neural networks do not generalize naturally when segmenting cine-MRI images with distinct imaging domains [3]. The lack of generalizability of neural networks to unseen domains limits their clinical applicability at scale. Thus far, several approaches have been attempted to address this problem in non-contrast imaging, such as methods based on extensive spatial- and intensity-based data augmentation [4], the use of synthetic images from generative models [5], explicit domain adaptation (by forcing the model to learn a similar representation across domains) [6, 7, 8], transfer learning [9, 10] and meta-learning [11, 12]. However, it is unclear whether such approaches can improve generalizability in the case of complex imaging modalities, such as in contrast-enhanced imaging, which is the subject of this paper.

In many clinical applications, contrast-enhanced imaging is applied to further improve the visibility of internal body structures and lesions in MRI [13], Computed Tomography [14] or Ultrasound [15] imaging. For example, late gadolinium enhancement MRI (LGE-MRI) is an essential imaging modality for several applications such as angiography [16], neuroimaging [17], oncology [18], hepatology [19] and cardiology [20]. Contrast-enhanced imaging is faced with additional challenges, compared to non-contrast imaging, due to the intensity heterogeneity arising from the accumulation of the contrast agent in the target areas and the artifacts introduced, which reduce the quality of the images and modify the data distributions. Furthermore, the time between contrast injection and image acquisition can vary greatly between patients and centers, typically between 7 minutes up-to to a total of 10 minutes, resulting in differences in contrast wash-out and image formation. As a result, the final image appearance, both globally and locally, can have marked differences as clearly illustrated in Figure 1 based on images from four different hospitals. At the same time, the limited numbers of available LGE-MRI datasets in existing open-access cohorts compared to non-contrast MRI images, combined with legal and organizational obstacles across centers and countries, has made access to interoperable multi-center LGE-MRI datasets more difficult. Hence, there is a need for new tools for generalizing single-domain, single-center deep learning models across new unseen domains and clinical centers in contrast-enhanced imaging such as in LGE-MRI.

1.2. Goals and contributions

In this paper, we present an exhaustive evaluation of deep learning techniques to achieve generalizability to unseen clinical centers for contrast-enhanced imaging. To this end, several techniques are investigated, optimized and systematically evaluated, including data augmentation, domain mixing, transfer learning and domain adaptation. To demonstrate the potential of domain generalization for contrast-enhanced imaging, the methods are evaluated for ventricular segmentation in cardiac LGE-MRI [21]. For this important clinical application, existing deep learning techniques have been almost systematically trained and validated with an LGE-MRI sample from a single clinical center ([22, 23, 24, 25]). As a result, while many research and commercial tools are already in use for non-contrast cardiac MRI, image segmentation in cardiac LGE-MRI still relies on labor-intensive manual delineation in clinical practice. Our work is based on a unique multi-center cardiac LGE-MRI dataset acquired with three distinct scanner vendors (Siemens, Philips and General Electric) in four hospitals located in three countries (France, Spain and China).

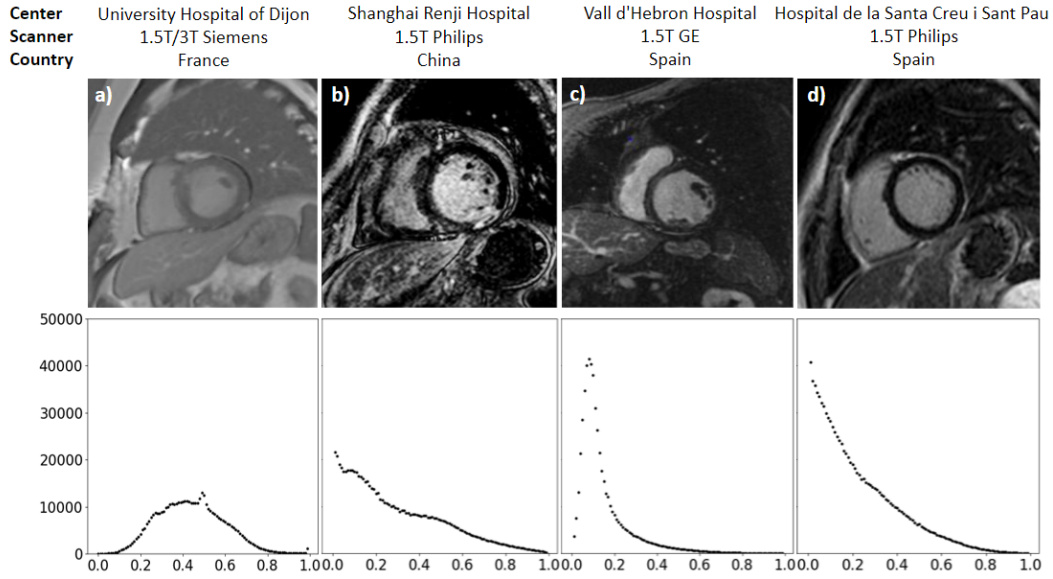


Figure 1: Four LGE-MRI cardiac images acquired in four different hospitals, together with the average intensity distribution of each dataset. Each histogram has a very different shape and shows marked variability between centers in terms of intensity distributions.

2. Methods

In this section, an end-to-end pipeline is investigated for generalizable image segmentation in multi-center LGE-MRI datasets. It is applied for deep learning-based segmentation of the left ventricle (LV), including the blood pool and the myocardium, in multi-center LGE-MRI cardiac images. To this end, four different approaches are explored to enhance the generalizability across clinical sites of existing deep neural networks for LGE-MRI segmentation, as schematically represented in Figure 2. These include:

1. Data augmentation techniques to artificially extend the data distribution captured by the trained models.
2. Image harmonization to align the data distributions of the training and testing images.
3. Transfer learning to adjust the neural network to the new clinical center based on very few unseen images.
4. Multi-center models directly trained with data from multiple clinical centers, which are used for comparative evaluation of the different generalization mechanisms.

We confirm that all experiments were performed in accordance with relevant guidelines and regulations.

2.1. Datasets

The multi-center and multi-vendor dataset used in this study consists of 216 cardiac LGE-MRI datasets acquired in four different clinical centers as detailed in Table 1. Two out of four samples are publicly available datasets from France and China, while the two other samples correspond to new LGE-MRI images acquired in two different hospitals in Spain. The subjects have been scanned by using a range of scanner vendors by Siemens, Philips or General Electric (GE). In addition to

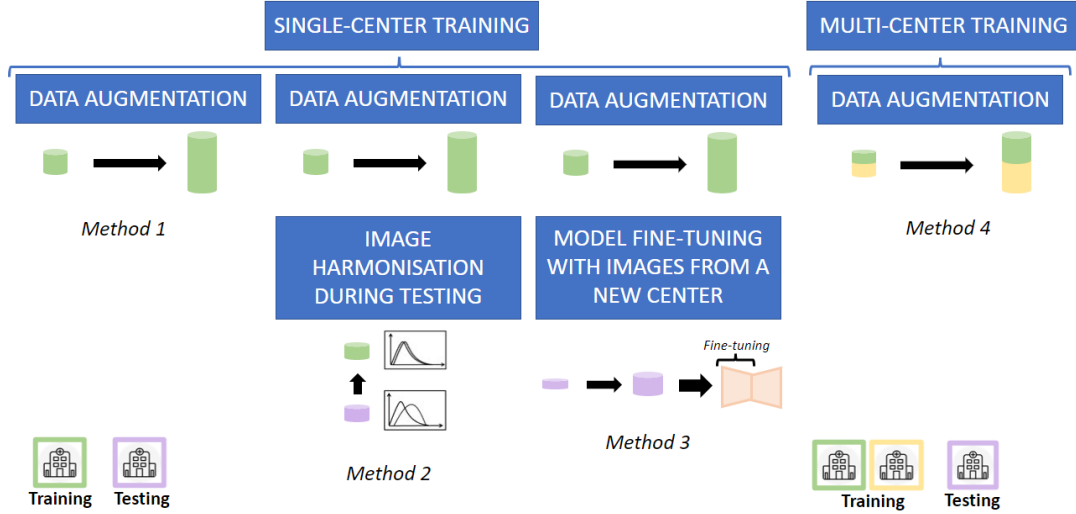


Figure 2: Four different approaches implemented in this work to enhance the generalisability of LGE-MRI segmentation models across distinct clinical sites.

Table 1: Details of the multi-center LGE-MRI datasets and characteristics of the acquired images used in this work. Imaging time = Acquisition time after contrast injection.

Dataset	Clinical center	Country	MRI scanner	Imaging time (mins)	In-plane resolution (mm)	Slice thickness (mm)	Number of slices	Sample size
EMIDEC	University Hospital of Dijon	France	1.5T and 3T Siemens	10	1.37-1.88	8-13	4-10	100
MSCMR	Shanghai Renji Hospital	China	1.5T Philips	-	0.75	5	10-18	45
VH	Vall d'Hebron Hospital	Spain	1.5T GE	10	1.48-1.68	10	8-15	41
STPAU	Sant Pau Hospital	Spain	1.5T Philips	7-10	1.18	5	18-24	30

having distinct intensity distributions as observed in Figure 1, the multi-center LGE-MRI images also differ in the image resolution (0.75-1.88 mm), slice thickness (5-13 mm), and acquisition time after contrast injection (7 to 10 minutes). The samples from each clinical site are described in more detail in the next subsections.

2.1.1. EMIDEC dataset: University Hospital Dijon, France

This dataset was compiled as part of the automatic Evaluation of Myocardial Infarction from Delayed-Enhancement Cardiac MRI challenge (EMIDEC) [26]. The EMIDEC volunteers included 33 healthy and 67 diseased subjects, for a total of 100 studies. The data was acquired at the University Hospital of Dijon, France, using Area 1.5 T as well as Skyra 3T Siemens MRI scanners. Slice thickness and in-plane spatial resolution varied greatly, being comprised between 8 and 13 mm and 1.37 and 1.88 mm, respectively. The manual segmentation of the LV blood pool and myocardium were performed by a cardiologist with over 10 years of experience. It is the largest of the four samples and hence it was used as the reference sample for training the single-center neural networks.

2.1.2. MSCMR dataset: Shanghai Renji Hospital, China

The MSCMR dataset was obtained from the Multi-sequence Cardiac MR Segmentation Challenge and it comprises a total of 45 patients suffering from various cardiomyopathies ([27], [28]). The images were acquired at the Shanghai Renji hospital, China, which will allow us to evaluate generalizability across countries as well as continents in this study. Compared to EMIDEC, the MSCMR dataset has a higher image resolution (in-plane resolution = 0.75 mm, slice thickness = 5 mm for all scans) and all images were acquired with a 1.5 T Philips scanner. The manual delineations were initially performed by trainees and later on validated by expert cardiologists.

2.1.3. VH dataset: Vall d'Hebron Hospital, Spain

The VH dataset consists of 41 LGE-MRI datasets acquired at the Vall d'Hebron University Hospital, located in Barcelona, Spain. In addition to covering a new geographical location, namely Spain, the VH sample has several differences with EMIDEC and MSCMR, including the disease group (MI) and the MRI scanner (1.5 T GE scanner). Manual annotations of the LV boundaries were generated by a trained rater using the cvi42 software. The study was approved by the ethics committee of the Vall d'Hebron Hospital and written informed consent was obtained from all participants.

2.1.4. STPAU dataset: Sant Pau Hospital, Spain

The STPAU dataset comprises 30 LGE-MRI cases acquired at the Sant Pau Hospital in Barcelona, Spain. While the clinical center is located in the same region as for the VH sample, the dataset covers a different disease group (ischemic and non-ischemic cardiomyopathy) and was acquired using an MRI scanner from a different vendor (Philips Achieva 1.5T) and a higher-resolution imaging protocol. Furthermore, the time delay between contrast injection and image acquisition varies between 7 and 10 minutes, which adds extra variability. The manual annotations were also performed using cvi42, as in the previous case. All patients signed the informed consent, the study protocol was approved by the Ethical Committee for Clinical Research of our region, and it follows the ethical guidelines of the Declaration of Helsinki.

2.2. Single-center model with data augmentation

In this work, we first investigate the potential of data augmentation to enhance the generalizability of LGE-MRI segmentation models (Method 1 in Figure 2). Data augmentation has been widely used to create more robust neural networks by increasing the size as well as the heterogeneity of training samples synthetically. However, the promise of data augmentation is yet to be examined for LGE-MRI, where there is higher complexity due to inherent variability in scar characteristics and contrast appearance.

In this work, we investigate several operators for data augmentation in the context of LGE-MRI as illustrated in Figure 3 and described as follows.

1. **Spatial-based data augmentation:** In addition to the natural variability between cardiac anatomies, especially across countries and ethnic groups, patients undergoing LGE-MRI typically suffer from regional remodelling of the ventricles due to the presence of scar tissue. Hence, spatial-based data augmentation is proposed using the following operators:
 - Horizontal and vertical flips to generate images with different orientations.
 - Random rotations of up to ± 30 degrees, to simulate different positions of the heart.
 - Random rescaling in the $[0.75, 1.88]$ mm range so that the model can process images and hearts that vary in size. This range is defined by the minimum and maximum voxel size of our multi-center dataset.

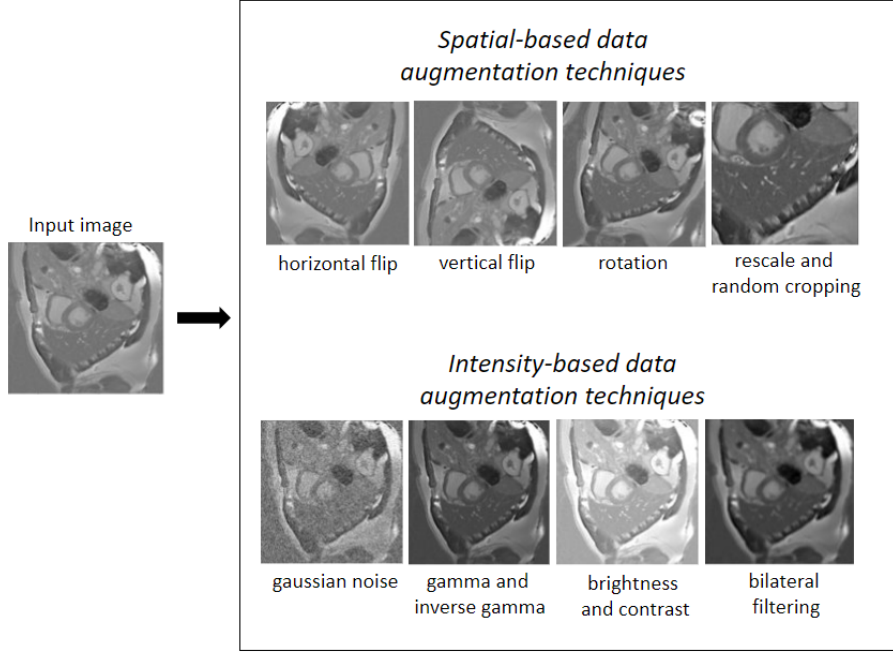


Figure 3: Both spatial and intensity-based data augmentation techniques are applied together with a probability of 0.2 each. From only one slice many samples can be generated, increasing the size of the original dataset significantly.

- Random cropping, such that the training images have the same dimensions of 256x256 pixels but with a variation in the position of the heart in the image.
2. **Intensity-based data augmentation:** Because the LGE-MRI appearance can vary between images acquired using different MRI scanners and scanning protocols, such as due to differences in acquisition time after contrast injection, we implemented the following intensity-based data augmentation techniques:
- Bilateral filtering to generate blurred and less detailed copies of the original images.
 - Gaussian noise with a standard deviation ranging between $[0, 0.03]$ to generate artificial noise and image artifacts.
 - Gamma and inverse Gamma function with magnitude $[0.7, 1.5]$ to generate synthetic images with different lighting.
 - Brightness and contrast with magnitude $[-0.5, 0.5]$ to support brightness and contrast variations in the training images.

Each data augmentation technique is applied with a probability of 0.2 during the training of the model. Then, this data augmentation pipeline is evaluated by measuring the final generalization ability of the network (Method 1 in Figure 2). Table 2 summarizes the split of the data used for the training, validation and testing of the model in each experiment.

2.3. Image harmonization at testing

While the data augmentation operations focused on improving model generalizability at training, we propose to apply image harmonization at the testing stage to further reduce the discrepancies

Table 2: Number of subjects for each of the four datasets used during the training, validation and testing phases when data augmentation is implemented in a single-center setting.

Dataset	Training	Validation	Testing
EMIDEC	68	17	15
MSCMR	24	6	15
VH	21	5	15
STPAU	12	3	15

Table 3: Number of samples used for the training and validating each CycleGAN model built to harmonise the imaging properties from the different clinical centers.

Dataset		Training		Validation	
Source	Target	Source	Target	Source	Target
EMIDEC	MSCMR	24	24	6	6
EMIDEC	VH	21	21	5	5
EMIDEC	STPAU	12	12	3	3
MSCMR	VH	21	21	5	5
MSCMR	STPAU	12	12	3	3
VH	STPAU	12	12	3	3

between the multi-center LGE-MRI images (Method 2 in Figure 2). Image harmonization enables to transform the testing LGE-MRI images from a new clinical center such that their intensity distribution matches as much as possible the imaging characteristics of the single center used to train the baseline neural network. Concretely, two main image harmonization techniques were implemented:

1. **Histogram matching:** It consists of transforming the testing images from the unseen center such that the histogram of the pixel intensity values is superimposed as much as possible with the corresponding histogram extracted from the training images from the training clinical center. The transformation from the testing data (B: target data) to the training data (A: source data) is illustrated in Figure 4(i).
2. **CycleGAN:** Another strategy to address the domain shift between multiple centers is domain adaptation, which can be used to learn the image translation from the source domain to the target domain. To this end, we choose to implement a CycleGAN architecture [29], based on an unpair image-to-image translation. Given that CycleGAN uses cycle consistency, it would learn the translation from the target domain (B) to the source domain (A), and viceversa (Figure 4(ii)). Both target to source and source to target generators are saved in each implementation, decreasing to 6 the number of implementations needed. The amount of samples used to train each of the CycleGAN models are summarised in Table 3, adjusting for each case the percentage of images from each center so that it is adequately balanced (50% source and 50% target data).

2.4. Transfer learning from the original to the new clinical site

Another strategy investigated in this work to improve the scalability of single-center models consisted of applying the so-called transfer learning paradigm, by fine-tuning specific layers of the neural network with a reduced number of LGE-MRI images from the new clinical site (Method 3 in Figure 2). The approach has shown promise for multi-center image segmentation in cardiac

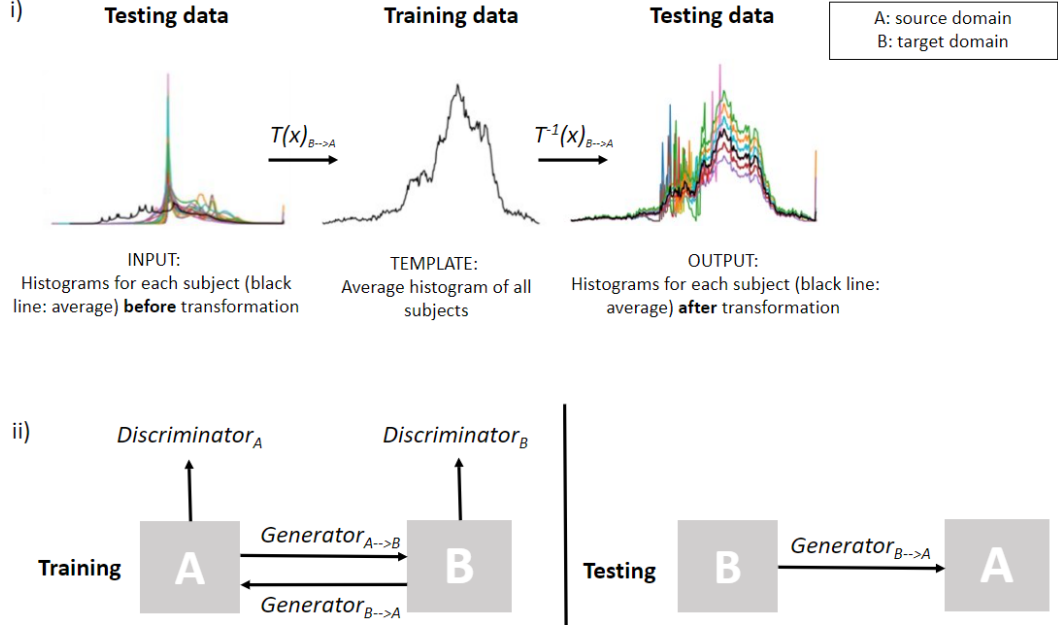


Figure 4: Schematic illustration of the image harmonisation techniques used in this work to make the intensity distributions from the different clinical sites as aligned as possible. First, histogram matching is used to learn a transformation of the histogram of each image from the unseen clinical sites (B) onto the original training clinical center (A). Second, CycleGAN architecture is used to learn the mapping between the training and the testing clinical center.

cine-MRI [30], but is yet to be demonstrated for multi-center LGE-MRI imaging, where there is increased variability. The following steps are implemented in this work:

1. Initiate the training of the neural network with the EMIDEC dataset, then evaluate the minimum number of fine-tuned layers, in both the decoder and the encoder, that are needed during transfer learning to obtain the maximal segmentation performance on the new LGE-MRI datasets from the remaining clinical centers.
2. Compare the previous results with the segmentations obtained based on a multi-center model directly trained each time with images from two clinical centers (EMIDEC and the new center).
3. Estimate the minimum percentage of images needed from the second clinical center during the fine-tuning to obtain the desired level of performance.
4. Implement the same approach from the previous point but this time by using a model pre-trained on a large dataset ($n=350$) from cine-MRI (M&Ms dataset), to evaluate transfer learning from a related cardiac MRI modality for which data is abundantly available.

2.5. Multi-center model

A fourth and last modelling strategy, i.e. training the neural networks directly from multiple centers (Method 4 in Figure 2), is used for comparative evaluation of the three extended single-center models described in the previous section, i.e. enriched with data augmentation, image harmonization and transfer learning. In this study, we investigated the amount of new centers/domains that are needed to bridge the domain gap in LGE-MRI segmentation, by using a balanced dataset with the same number of subjects for each multi-center data combination, namely

Table 4: List and number of samples used for training and validating multi-center models in this study.

Dataset	Training	Validation
EMIDEC	42	10
EMIDEC+MSCMR	21+21	5+5
EMIDEC+VH	21+21	5+5
EMIDEC+MSCMR+VH	14+14+14	3+3+3
EMIDEC+MSCMR+VH+STPAU	11+11+11+11	3+3+3+3

EMIDEC, EMIDEC+MSCMR, EMIDEC+VH, EMIDEC+MSCMR+VH and ALL centers. The samples used for training the multi-center models in each combination of datasets/centers are listed in Table 4. In all experiments, the same testing dataset is used for comparative evaluations (n=15).

2.6. Baseline workflow

2.6.1. Pre-processing

Min-max normalization is used after cropping of the image to keep the same intensity range in images from the same dataset.

2.6.2. Post-processing

A post-processing is applied to all predictions generated by the model by keeping only the largest connected component of the segmentation volume. This step is commonly used in medical image segmentation, especially in organ imaging, to help on the detection of false positives.

2.6.3. Network architecture

As a baseline model, a U-Net architecture is implemented to perform the LV boundary segmentations in LGE-MRI based on some of the modifications proposed by [31] for improved model training as follows. First, Leaky ReLU is used as activation function, then instance normalization is applied after each hidden convolutional layer to stabilise the training. Deep supervision is included to allow gradients to be injected deeper into the network and facilitating the training of all layers. Furthermore, a 2D architecture is selected as it is suitable to address the differences in slice thickness between clinical centers, as well as slice misalignment due to respiratory and cardiac motion artefacts. The encoder and decoder architecture of the model are illustrated in Figure 5.

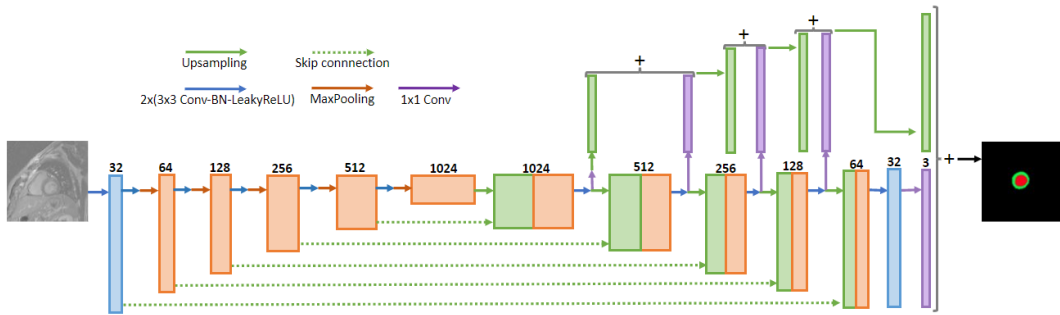


Figure 5: U-Net architecture composed by 6 layers, increasing progressively the number of feature maps until 1024. Additionally, deep supervision layers are included in the decoder.

Table 5: Dice score coefficient for the different domain generalization experiments performed. The results are averaged over five runs of models. All models used EMIDEC for training. In experiment 3, every model is transferred to the corresponding target center and in experiment 4, every model is trained with EMIDEC and a training set from the corresponding target center. Standard deviation is presented as subscript for five independent runs of each model.

Test Center	<i>Experiment 1</i> Effect of data augm. (single-center training)			<i>Experiment 2</i> Image harmonization		<i>Experiment 3</i> Transfer learning	<i>Experiment 4</i> Multi-center training
	No augm.	Spatial	Spatial & intensity	CycleGAN	Hist. match.		
EMIDEC	0.85 _{0.05}	0.88 _{0.03}	0.78 _{0.08}	-	-	-	-
MSCMR	0.30 _{0.15}	0.62 _{0.19}	0.72 _{0.12}	0.64 _{0.17}	0.78 _{0.07}	0.87 _{0.03}	0.89 _{0.03}
STPAU	0.54 _{0.16}	0.61 _{0.12}	0.68 _{0.09}	0.70 _{0.08}	0.68 _{0.08}	0.85 _{0.04}	0.85 _{0.04}
VH	0.32 _{0.21}	0.26 _{0.23}	0.62 _{0.13}	0.53 _{0.17}	0.58 _{0.12}	0.78 _{0.11}	0.82 _{0.06}

2.6.4. Implementation details

PyTorch is the open-source machine learning library for Python used for the implementation of the model learning. Stochastic gradient descent (SGD) optimization is performed with Adam and the batch size of 16 slices is constrained by the 8 GB of memory of the NVIDIA GeForce RTX 2080 Ti GPU. The learning rate is kept to $1 \cdot 10^{-3}$ during every training, while the dice and cross entropy losses are calculated at every iteration to optimize the network parameters. The neural network is trained 250 epochs each time and takes half an hour approximately to converge. During testing, each LGE-MRI image segmentation takes less than one second. The main criterion followed to split each dataset in subgroups is 80% for the training and 20% for the validation part, while keeping 15 subjects for the testing.

2.6.5. Performance evaluation

For all experiments and results, the performance of each method will be assessed with the average 3D Dice Coefficient (DC), which calculates the overlap ratio between the automatically generated and ground truth segmentations. The measure is estimated by:

$$DC = \frac{2 \cdot (X \cap Y)}{X + Y} = \frac{2 \cdot TP}{2 \cdot TP + FP + FN}, \quad (1)$$

where X and Y are the set of pixels from the automated and true labels of the target structures, while TP, FP, and FN are the corresponding true positives, false positives and false negatives, respectively.

3. Results

This section presents detailed experimental results obtained by evaluating and comparing the different strategies proposed for enhancing model generalizability in LGE-MRI segmentation. Four experiments are proposed to study model generalizability: (1) effect of data augmentation, (2) image harmonization, (3) transfer learning and (4) multi-center training. The results are summarized in Table 5, where a similar limited generalization performance is achieved for experiments (1) and (2) while experiments (3) and (4) show a significant improvement. Each experiment is analyzed in detail next.

3.1. Experiment 1: Effect of data augmentation

In the first experiment, the added value of the different types of data augmentation is evaluated, including spatial and intensity-based data augmentations. Figure 6 shows the comparative results obtained by three different models: (i) a single-center model without data augmentation (blue line), (ii) a single-center model with spatial data augmentation (orange), and (iii) a single-center model enriched with both spatial and intensity based data augmentations (green). As observed in the results, data augmentation consistently improves the segmentation performance for LGE-MRI independently of the clinical center used for training, increasing the DC value up to 0.6 units with respect to the baseline model without data augmentation. Furthermore, the results in Figure 6 show that while most of the improvement can be achieved by spatial data augmentation (orange line), intensity-based data augmentation adds value to the approach, in particular when training on the largest sample (EMIDEC) and testing on smaller samples (MSCMR, VH and STPAU). Having demonstrated the added value of data augmentation, all subsequent experiments are performed using spatial- and intensity-based data augmentation.

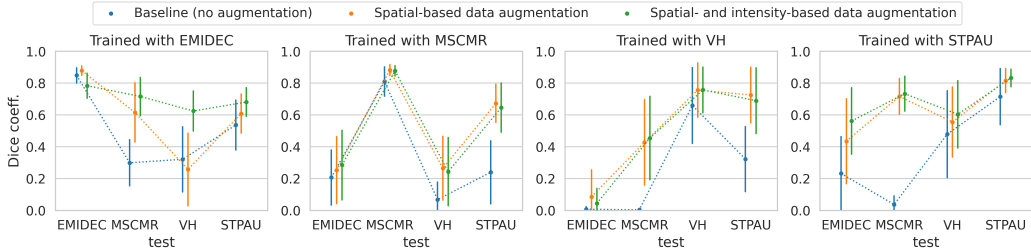


Figure 6: Comparison of the subject-wise Dice coefficient obtained for models trained with a single-center with and without data augmentation, including spatial- and intensity-based augmentations. Models are tested on subjects from the testing set for every center. The results are averaged over five different runs of each model.

3.2. Experiment 2: Effect of image harmonization

Here, the impact of image harmonization is evaluated when applied to match the intensity distribution and appearance of LGE-MRI images from a new clinical center to that of the training set. Specifically, we evaluate three approaches, namely (i) the baseline model with data augmentation from Experiment 1 but without any normalization, (ii) the baseline model with histogram matching, and (iii) the baseline model with CycleGAN normalization. The results are given in Figure 7, clearly showing that, overall, the two harmonization operations (green and orange lines) do not improve significantly the LGE-MRI segmentations over the baseline model without harmonization (blue line). There are, however, few cases where the mean Dice score is slightly improved, as for histogram matching when training with EMIDEC and testing in MSCMR or when using CycleGAN for models trained with VH.

3.3. Experiment 3: Effect of transfer learning

This section evaluates the potential value of fine-tuning a model pre-trained on a larger dataset (such as EMIDEC) via transfer learning and the effect of the sample size used during the tuning process. Figure 8 shows the performance of transfer learning for a model pre-trained with EMIDEC and fine-tuned for each new clinical center (MSCMR, VH and STPAU). The red and blue lines in the figure show the segmentation accuracy when the fine-tuning is performed on the encoder and decoder of the neural network, respectively, while the remaining parts of the model are frozen. The black

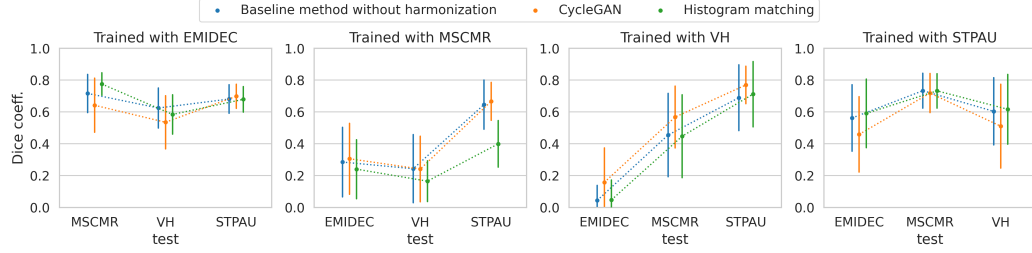


Figure 7: Effect of histogram matching and CycleGAN harmonisation for LGE-MRI segmentation in unseen clinical centers. X corresponds to each testing center not included in the training dataset and the results are averaged over five different runs of each model.

line corresponds to a model trained and tested on the same center. The results show an increase in DC with the number of fine-tuned blocks and the maximum is obtained when 5 or all blocks of the encoder are fine-tuned, reaching nearly the same performance as the single-center model of the new center (black line). Furthermore, in Figure 9, the single-center models fine-tuned based on 5 encoding blocks are directly compared to multi-center models trained based on all images from the original and new clinical centers. Based on the results, fine-tuned models (green bars) –despite being fine-tuned on the new LGE-MRI images– achieve similar segmentation performances than models directly trained from multi-center image data (orange bars). This shows the potential of transfer learning to adjust and optimize a few layers of the existing single-center model based on unseen LGE-MRI images from a new clinical center.

However, transfer learning requires manual annotations of some images from the new clinical sites. Hence, ideally the number of new annotated images required to suitably adapt the existing model to the new center should be minimal. In Figure 10, we evaluated the impact of the number of new LGE-MRI images used for fine-tuning. The results indicate that the fine-tuning of single-center models with a small percentage of the target data is sufficient to reach a desirable segmentation accuracy. Such generalization is achieved, for example, in the case of a single-center model pre-trained with the EMIDEC dataset and fine-tuned using only 10% (about 1-3 subjects) from the new dataset. A similar pattern is found when training with a different modality, as shown by the model pre-trained with cine-MRI images from the M&Ms dataset (gray line), except for a better performance when testing on the VH center.

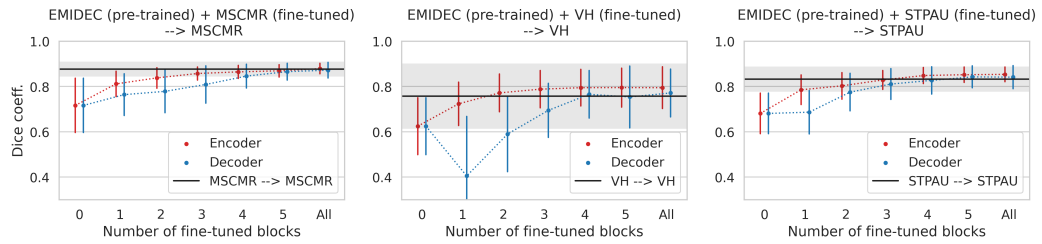


Figure 8: Evaluation of a single-center model pre-trained on the EMIDEC dataset and fine-tuned with a new clinical dataset (MSCMR, VH or STPAU). Red: Fine-tuning of a number of blocks in the encoder. Blue: Fine-tuning of a number of blocks in the decoder. Black: Model trained from scratch with data from the same center. Bars and gray band stand for the standard deviation of the five independent model runs.

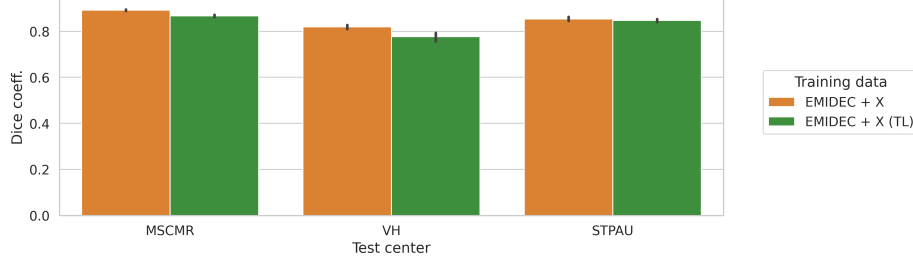


Figure 9: Model trained from scratch using EMIDEC and a second dataset (X), which can be MSCMR, VH or STPAU (orange). Then, a model pre-trained with EMIDEC, and fine-tuned and evaluated on X (green). The black bars represent the standard deviation for five independent runs of each model. TL: transfer learning.

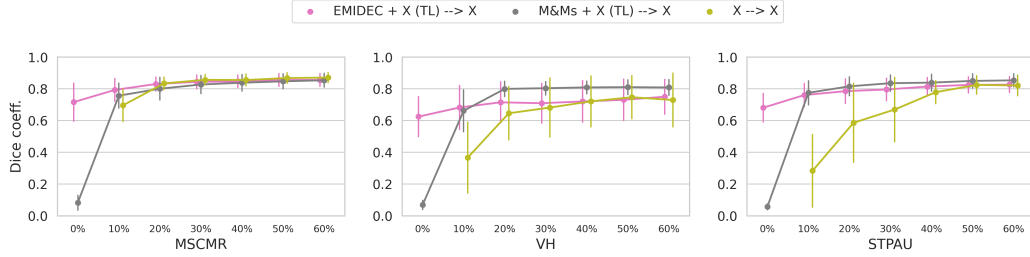


Figure 10: Impact of sample size (percentage) of a new LGE-MRI dataset used for fine-tuning existing single-center models for different training datasets (fuchsia and gray) and compared to single-center models (yellow). Results are averaged over five independent model runs.

3.4. Experiment 4: Comparison to a multi-center scenario

In this last experiment, the added value of training multi-center models for LGE-MRI segmentation is evaluated by including training images from multiple clinical sites (i.e. from 1 to 4 centers). In Figure 11 different combinations of the four datasets considered in this study were explored, either by using a baseline model, data augmentation or histogram matching. As observed in the results, when the model is trained with no data augmentation (baseline), the multi-center data enhanced the generalization ability as demonstrated by the increase in average DC values and the reduction of the standard deviation. However, when data augmentation is included in the pipeline, no gain is found by adding new clinical sites to the training stage, as the data augmentation alone is sufficiently powerful for training the model with reduced over-fitting when tested in new centers. The results also confirm that histogram matching does not show significant positive impact on the final performance.

3.5. Qualitative analysis

Finally, we show a qualitative comparison in Figure 12 of model predictions (colored overlay) for selected cases that demonstrate the common mistakes of the models as compared to the groundtruth (white delineations). For instance, the first three columns show how data augmentation improves the model ability to identify and segment the left ventricle while for some cases (like for the second row, with the VH sample), it is still insufficient. The fourth and fifth columns show the effect of the image harmonization experiments, which help in segmenting failing cases but do not improve significantly the accuracy of the segmentation as observed in the disagreement between groundtruth

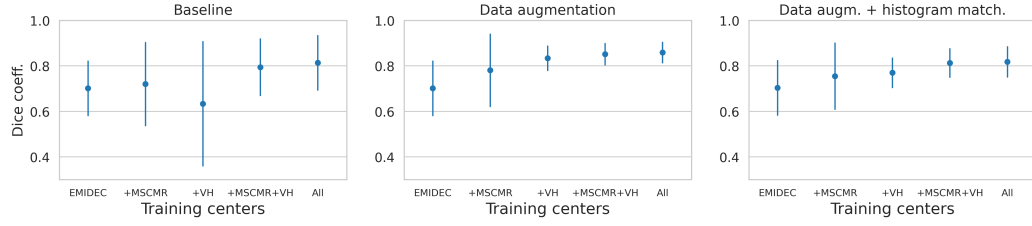


Figure 11: Average DC achieved by models trained on different combinations of clinical datasets, with and without data augmentation, as well as with histogram matching. The first model is initially trained with the EMIDEC dataset, and then new datasets are included progressively from the three other clinical sites. Results are averaged over five independent model runs.

and predictions. Finally, the last two columns show the predictions for transfer learning and multi-center models, respectively. These final predictions are the most accurate among all the columns, but one can still identify some disagreements in challenging regions annotated with orange arrows where scars can be found.

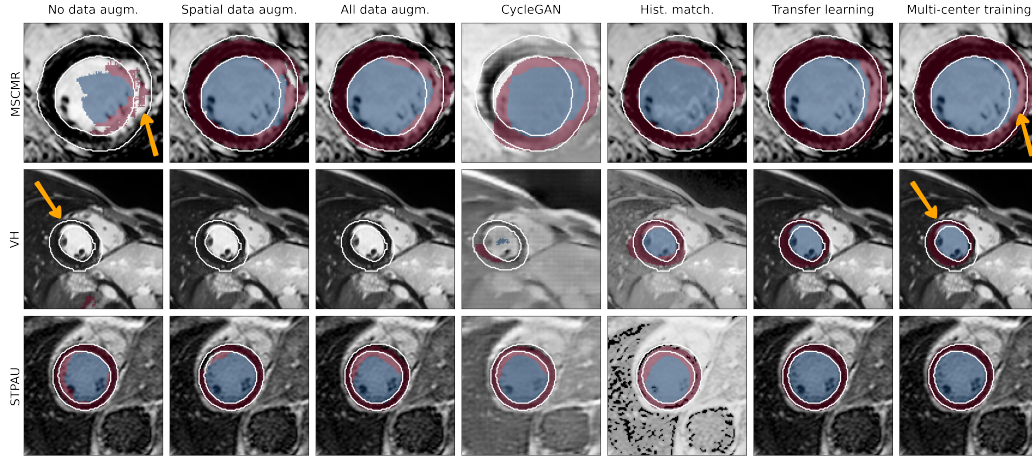


Figure 12: Qualitative comparison of model predictions for selected slices of test subjects. The groundtruth is delineated with white lines while the overlaid color represents the model prediction. Each row corresponds to a different dataset and each column corresponds to each model as presented in Table 5. Challenges regions with scars are highlighted with orange arrows in the first and last columns.

4. Discussion

In this work several strategies were implemented and evaluated for generalizable segmentation of left ventricular anatomy in multi-center LGE-MRI. The pipeline was built with the purpose to train single-center models that can maintain a good level of performance when used to segment out-of-sample images from new hospitals. The results highlight the importance of using data augmentation, including both spatial and intensity-based transformations, in particular when there is a high domain shift between the training and unseen clinical site, e.g. EMIDEC in our results. After applying adequate data augmentation to existing single-center models, it was found that neither multi-center

training nor image harmonization techniques are needed to obtain additional generalizability, confirming the results obtained by [3] in the M&Ms study for a multi-center and multi-vendor cine-MRI. This finding shows that single-center LGE-MRI models can generalize well if appropriately enriched with data augmentation, which results in an important practical benefit: Multi-center training is difficult in practice as there is a lack of labelling harmonization between centers, in addition to the legal and other obstacles that make difficult cross-site data sharing. Moreover, multi-center models are still specific to those clinical centers that contributed data, whereas there is need for models that can generalize well beyond the training data.

Regarding domain adaptation, which theoretically is a promising solution, existing research has shown that histogram matching could lead to hidden noise in some images after the post-processing [32], while CycleGANs would typically require substantial training data from the new clinical center to achieve a good model performance. In addition to data augmentation, the results demonstrated that transfer learning can positively impact the model performance across sites. This method is based on the fine-tuning of an existing model initially pre-trained on a single-center dataset and adjusted with few datasets from the new clinical site. The obtained results indicate that fine-tuning the first 5 blocks of the encoder of the model with the 10% of the dataset, ranging from 1 to 3 subjects, is sufficient to achieve the desired LV segmentation accuracy in LGE-MRI. For example, a neural network pre-trained based on the EMIDEC dataset and fine-tuned with one subject/image only from STPAU (DC: 0.76 ± 0.07) performs similarly when compared to a model trained from scratch with the 100% of the STPAU images (DC: 0.79 ± 0.13). In terms of computational time, the first model is completely trained in half an hour and the posterior fine-tuning requires only 5 minutes.

In addition to transfer learning focused on LGE-MRI, we evaluated the potential of fine-tuning a pre-existing model trained on larger cine-MRI datasets from the M&Ms dataset, which consists of a 350 training images. Despite the different imaging characteristics between cine and LGE-MRI images, in particular the additional presence of scar tissue and contrast enhancements in the LGE-MRI images, the results showed that such cross-modality transfer learning results in enhanced generalizability. This can be easily explained by the fact that such pre-trained multi-center and multi-disease model encodes additional inter-subject variability which aids generalizability also in multi-center and multi-disease LGE-MRI context.

Finally, to illustrate the success of data augmentation and transfer learning to build models with good generalization ability, Figure 13 provides two examples of challenging LGE-MRI cases, with varying imaging and anatomical characteristics. Despite the fact that these images are from two different clinical centers and vary greatly in the appearance, size, shape and location of the scar tissues, the proposed enriched models are capable to accurately identify the LV boundaries consistently across the LGE-MRI examples.

Compared to other multi-center existing studies, such as the M&Ms challenge that comprises 350 cine-MRI cases, the present multi-center LGE-MRI study has a lower sample size. This is because the LGE-MRI datasets are less abundant and more difficult to compile for research studies. Nevertheless, the results in this work are generated based on 216 datasets from four clinical centers, three vendors (Siemens, Philips and GE) and three countries from two different continents.

Another limitation is that this work was focused on the segmentation of the LV anatomy and did not consider the more challenging task of segmenting the scar tissues. This is due to the fact that the clinical annotations for the scar tissues were not available for the two clinical centers in Spain. Future multi-center studies in LGE-MRI should also investigate generalizability of neural networks for scar tissue segmentation. However, our work is an important first step in this direction, and one that will encourage the development of more generalizable models based on data augmentation and transfer learning, in LGE-MRI but also in other cardiac and non-cardiac imaging modalities.

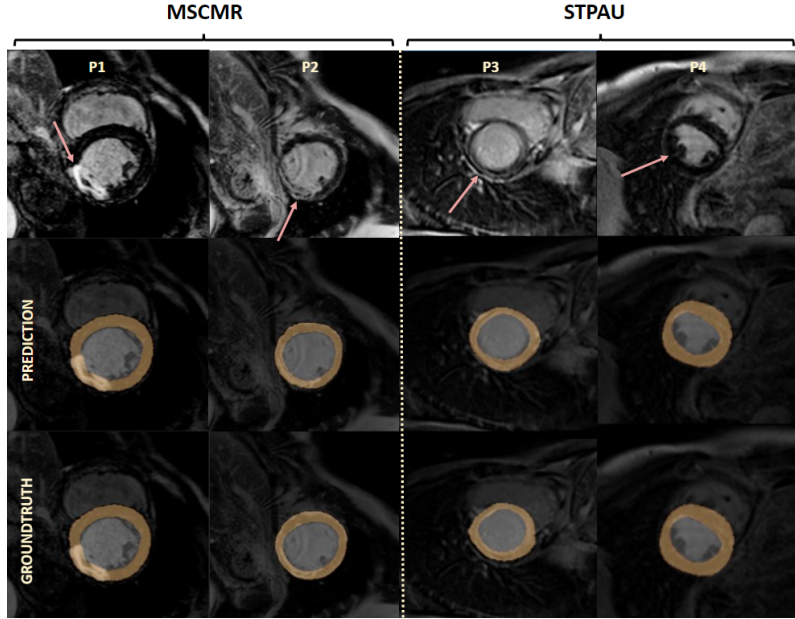


Figure 13: Challenging cases leading to good model predictions on two patients from two different hospitals. First row: original image, second row: prediction, third row: groundtruth. Each of the two columns correspond to images obtained from MSCMR or STPAU datasets respectively. The red arrows highlight the infarct or scar tissue.

While the proposed framework shows promise for generalizability across multi-center LGE-MRI datasets with challenging and heterogeneous conditions, it can fail to accurately identify the LV boundaries in a few exceptions. As illustrated in Figure 14, a number of failures have been observed in the presence of low-quality images with artifacts due to suboptimal contrast wash-out or highly complex scar appearance. Furthermore as reported in previous works in cardiac cine-MRI segmentation [4], apical and basal slices are also more error-prone than mid-ventricle slices in LGE-MRI segmentation. In fact, even experienced cardiologists can disagree on the segmentation of the LV borders closer to the apex and base, which generates inter-operator variability that can confuse neural networks, as illustrated in Figure 15.

5. Conclusions

This work was motivated by the need for new deep learning based solutions that generalize well across domains, centers and scans, in non-contrast as well as in contrast-enhanced imaging. Data augmentation extended the image distribution in single-center settings and proved to be an effective technique to generate models with a prominent generalization ability to new clinical centers. In contrast, image harmonization did not improve the capability of single-center models when tested on unseen clinical sites. Furthermore, the exploitation of transfer learning based on fine-tuning of pre-trained models with as little as one additional subject from an unseen clinical site translated into a substantial improvement in the model’s generalizability. This paper showed that single-domain neural networks enriched with suitable generalization procedures can reach and even surpass the performance of multi-center, multi-vendor models in contrast-enhanced imaging, hence eliminating the need for comprehensive multi-center datasets to train generalizable models.

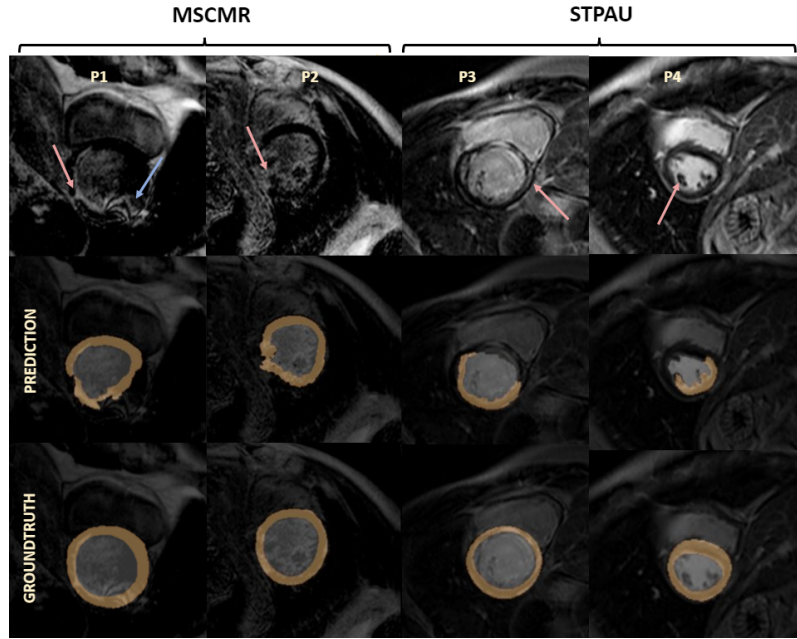


Figure 14: Segmentation failures obtained due to artifacts and highly complex scars. First row: original image, second row: prediction, third row: groundtruth. Each of the two columns correspond to images obtained from MSCMR and STPAU datasets respectively. The blue arrow shows an image artifact, while the red arrows points to the infarct or scar tissue.

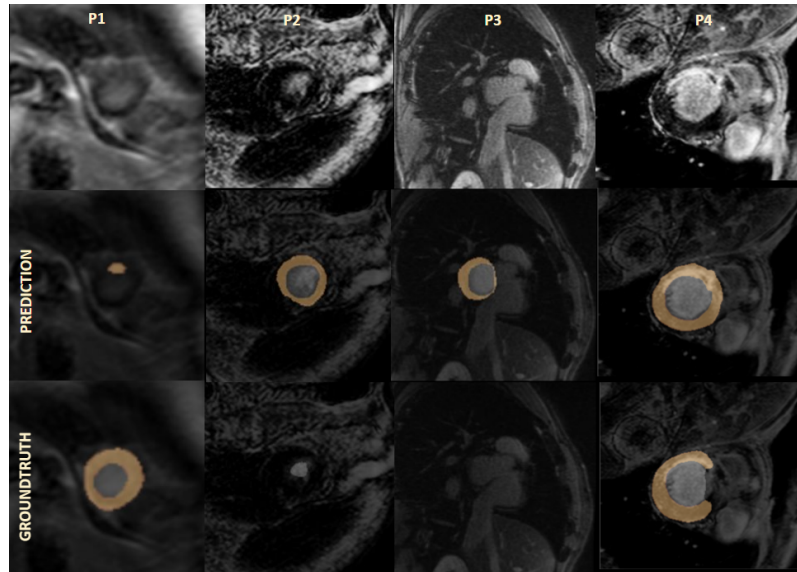


Figure 15: Examples of segmentation failures obtained at the apical and basal slices. First row: original image, second row: prediction, third row: groundtruth. First and second column show two similar cases where both apical slices are segmented differently. The third and forth columns are two heterogeneous segmentation at the basal region.

Funding

This work received funding from the European Union’s 2020 research and innovation programme under grant agreement No. 825903 (euCanSHare project), as well as from the Spanish Ministry of Science, Innovation and Universities under grant agreement RTI2018-099898-B-I00. Guala A. received funding from the Spanish Ministry of Science, Innovation and Universities (IJC2018-037349-I).

Abbreviations

Late gadolinium-enhanced magnetic resonance imaging (LGE-MRI); Left ventricle (LV); Magnetic resonance imaging (MRI).

Availability of data and materials

EMIDEC and MSCMR dataset are publicly available. The VH and STPAU datasets are available from the corresponding author upon reasonable request.

Competing interests

The authors declare that they have no competing interests.

Authors’ contributions

Design of the work: CSB, VMC, CMI, KL. Image collection: DVM, MLD, AG, JFRP. Interpretation of results: CSB, VMC, CMI, KL. Manuscript draft: CSB, KL. Manuscript review: VMC, CMI, AG, KL.

References

- [1] H. Guan, M. Liu, Domain adaptation for medical image analysis: a survey, *IEEE Transactions on Biomedical Engineering*.
- [2] C. Chen, C. Qin, H. Qiu, G. Tarroni, J. Duan, W. Bai, D. Rueckert, Deep learning for cardiac image segmentation: A review, *Frontiers in Cardiovascular Medicine* 7 (2020) 25.
- [3] V. M. Campello, P. Gkontra, C. Izquierdo, C. Martín-Isla, A. Sojoudi, P. M. Full, K. Maier-Hein, Y. Zhang, Z. He, J. Ma, et al., Multi-centre, multi-vendor and multi-disease cardiac segmentation: The m&ms challenge, *IEEE Transactions on Medical Imaging*.
- [4] C. Chen, W. Bai, R. H. Davies, A. N. Bhuva, C. H. Manisty, J. B. Augusto, J. C. Moon, N. Aung, A. M. Lee, M. M. Sanghvi, et al., Improving the generalizability of convolutional neural network-based segmentation on cmr images, *Frontiers in cardiovascular medicine* 7 (2020) 105.

- [5] F. Kong, S. C. Shadden, A generalizable deep-learning approach for cardiac magnetic resonance image segmentation using image augmentation and attention u-net, in: *Statistical Atlases and Computational Models of the Heart. M&Ms and EMIDEC Challenges*, Springer International Publishing, Cham, 2021, pp. 287–296.
- [6] M. Parreño, R. Paredes, A. Albiol, Deidentifying mri data domain by iterative backpropagation, in: *Statistical Atlases and Computational Models of the Heart. M&Ms and EMIDEC Challenges*, Springer International Publishing, Cham, 2021, pp. 277–286.
- [7] J. Corral Acero, V. Sundaresan, N. Dinsdale, V. Grau, M. Jenkinson, A 2-step deep learning method with domain adaptation for multi-centre, multi-vendor and multi-disease cardiac magnetic resonance segmentation, in: *Statistical Atlases and Computational Models of the Heart. M&Ms and EMIDEC Challenges*, Springer International Publishing, Cham, 2021, pp. 196–207.
- [8] C. M. Scannell, A. Chiribiri, M. Veta, Domain-adversarial learning for multi-centre, multi-vendor, and multi-disease cardiac mr image segmentation, in: *International Workshop on Statistical Atlases and Computational Models of the Heart*, Springer, 2020, pp. 228–237.
- [9] V. Cheplygina, I. P. Pena, J. H. Pedersen, D. A. Lynch, L. Sørensen, M. De Bruijne, Transfer learning for multicenter classification of chronic obstructive pulmonary disease, *IEEE journal of biomedical and health informatics* 22 (5) (2017) 1486–1496.
- [10] K. Kushibar, S. Valverde, S. González-Villà, J. Bernal, M. Cabezas, A. Oliver, X. Lladó, Supervised domain adaptation for automatic sub-cortical brain structure segmentation with minimal user interaction, *Scientific reports* 9 (1) (2019) 1–15.
- [11] X. Liu, S. Thermos, A. Q. O’Neil, S. A. Tsiftaris, Semi-supervised meta-learning with disentanglement for domain-generalised medical image segmentation, in: *MICCAI*, 2021.
- [12] C. Li, Q. Qi, X. Ding, Y. Huang, D. Liang, Y. Yu, Domain generalization on medical imaging classification using episodic training with task augmentation, *Computers in biology and medicine* 141 (2022) 105144.
- [13] D. Carr, J. Brown, G. Bydder, R. Steiner, H. Weinmann, U. Speck, A. Hall, I. Young, Gadolinium-dtpa as a contrast agent in mri: initial clinical experience in 20 patients, *American Journal of Roentgenology* 143 (2) (1984) 215–224.
- [14] A. Pepe, J. Li, M. Rolf-Pissarczyk, C. Gsaxner, X. Chen, G. A. Holzapfel, J. Egger, Detection, segmentation, simulation and visualization of aortic dissections: A review, *Medical Image Analysis* 65 (2020) 101773. doi:<https://doi.org/10.1016/j.media.2020.101773>.
- [15] C. Otto, *The Practice of Clinical Echocardiography*, ClinicalKey 2012, Elsevier/Saunders, 2012.
- [16] S. J. Riederer, E. G. Stinson, P. T. Weavers, Technical aspects of contrast-enhanced mr angiography: current status and new applications, *Magnetic Resonance in Medical Sciences* 17 (1) (2018) 3.
- [17] J.-C. Ferré, M. S. Shiroishi, M. Law, Advanced techniques using contrast media in neuroimaging, *Magnetic Resonance Imaging Clinics* 20 (4) (2012) 699–713.
- [18] N. Onishi, M. Sadinski, M. C. Hughes, E. S. Ko, P. Gibbs, K. M. Gallagher, M. M. Fung, T. J. Hunt, D. F. Martinez, A. Shukla-Dave, et al., Ultrafast dynamic contrast-enhanced breast mri may generate prognostic imaging markers of breast cancer, *Breast Cancer Research* 22 (1) (2020) 1–13.

- [19] C. L. Welle, F. F. Guglielmo, S. K. Venkatesh, Mri of the liver: choosing the right contrast agent, *Abdominal radiology* 45 (2) (2020) 384–392.
- [20] J. Uhlig, O. Al-Bourini, R. Salgado, M. Francone, R. Vliegenthart, J. Bremerich, J. Lotz, M. Gutberlet, Gadolinium-based contrast agents for cardiac mri: use of linear and macrocyclic agents with associated safety profile from 154 779 european patients, *Radiology: Cardiothoracic Imaging* 2 (5) (2020) e200102.
- [21] A. Doltra, B. Hoyem Amundsen, R. Gebker, E. Fleck, S. Kelle, Emerging concepts for myocardial late gadolinium enhancement mri, *Current cardiology reviews* 9 (3) (2013) 185–190.
- [22] Q. Yue, X. Luo, Q. Ye, L. Xu, X. Zhuang, Cardiac segmentation from lge mri using deep neural network incorporating shape and spatial priors, in: *International Conference on Medical Image Computing and Computer-Assisted Intervention*, Springer, 2019, pp. 559–567.
- [23] F. Zabihollahy, M. Rajchl, J. A. White, E. Ukwatta, Fully automated segmentation of left ventricular scar from 3d late gadolinium enhancement magnetic resonance imaging using a cascaded multi-planar u-net (cmput-net), *Medical physics* 47 (4) (2020) 1645–1655.
- [24] T. Kurzendorfer, K. Breininger, S. Steidl, A. Maier, R. Fahrig, Left ventricle segmentation in lge-mri using multiclass learning, in: *Medical Imaging 2019: Image Processing*, Vol. 10949, International Society for Optics and Photonics, 2019, p. 1094929.
- [25] X. Zhuang, J. Xu, X. Luo, C. Chen, C. Ouyang, D. Rueckert, V. M. Campello, K. Lekadir, S. Vesal, N. RaviKumar, et al., Cardiac segmentation on late gadolinium enhancement mri: a benchmark study from multi-sequence cardiac mr segmentation challenge, *arXiv preprint arXiv:2006.12434*.
- [26] A. Lalande, Z. Chen, T. Decourselle, A. Qayyum, T. Pommier, L. Lorgis, E. de la Rosa, A. Cochet, Y. Cottin, D. Ginjac, et al., Emidec: A database usable for the automatic evaluation of myocardial infarction from delayed-enhancement cardiac mri, *Data* 5 (4) (2020) 89.
- [27] X. Zhuang, Multivariate mixture model for cardiac segmentation from multi-sequence mri, in: *International Conference on Medical Image Computing and Computer-Assisted Intervention*, Springer, 2016, pp. 581–588.
- [28] X. Zhuang, Multivariate mixture model for myocardial segmentation combining multi-source images, *IEEE transactions on pattern analysis and machine intelligence* 41 (12) (2018) 2933–2946.
- [29] J.-Y. Zhu, T. Park, P. Isola, A. A. Efros, Unpaired image-to-image translation using cycle-consistent adversarial networks, in: *Proceedings of the IEEE international conference on computer vision*, 2017, pp. 2223–2232.
- [30] C. Ma, Z. Ji, M. Gao, Neural style transfer improves 3d cardiovascular mr image segmentation on inconsistent data, in: *International Conference on Medical Image Computing and Computer-Assisted Intervention*, Springer, 2019, pp. 128–136.
- [31] F. Isensee, P. F. Jaeger, S. A. Kohl, J. Petersen, K. H. Maier-Hein, nnu-net: a self-configuring method for deep learning-based biomedical image segmentation, *Nature Methods* 18 (2) (2021) 203–211.
- [32] P. Garg, T. Jain, A comparative study on histogram equalization and cumulative histogram equalization, *International Journal of New Technology and Research* 3 (9) (2017) 263242.